Molecular dynamics simulations of Lennard-Jones systems confined between suspended nanoscale graphene sheets

Norio Inui[*]

Graduate School of Engineering, University of Hyogo, Shosha 2167, Himeji, Hyogo 671-2201, Japan

The distribution of particles interacting with Lennard-Jones potentials and confined between parallel graphene sheets is investigated by molecular dynamics simulations. For small separation distances, the particles are densely localized in the central region between the graphene sheets. However, two high-density layers appear as the separation distance increases. The particle distribution also depends on the temperature, tensile force of the graphene sheets, and the initial configuration, and various configurations are observed for large separation. For example, an argon cluster initially located between the graphene sheets changes shape, and a bridge between the parallel walls is formed at low temperature. In contrast to the Lennard-Jones system sandwiched between rigid walls, the flexibility of the graphene sheets strongly affects the distribution of particles in the direction perpendicular to the graphene sheets.

I. INTRODUCTION

Interacting particle systems confined in a finite volume exhibit different behavior from those located in an unbounded space [1–4]. This finite-size effect is enhanced as the volume decreases and the interaction between the molecules and their surrounding surfaces becomes stronger. For example, molecules enclosed inside a carbon nanotube exhibit a unique behavior [5–7]. In this study, we model a Lennard-Jones system confined between nanographene sheets [8]. Despite their very small thickness, graphene sheets can prevent the permeation of molecules; in addition, owing to their very large Young modulus (almost 1 TPa) [9], they can seal high-pressure gas [10]. Thus, a narrow space between suspended graphene sheets is a good model for studying confined particles and two-dimensional (2D) Lennard-Jones systems [11]. Furthermore, since light and electron beams can penetrate graphene, molecules confined between graphene sheets may be detected using existing experimental techniques [12].

In this work, we focus on the dependence of the distribution of particles confined between two graphene sheets on the distance separating walls. In particular, we consider the effect of bending the graphene sheets on the particle distribution. The bending energy of a graphene sheet is very small compared with the stretching energy [13]: buckling of graphene sheets may occur by the interaction between the confined particles and the carbon atoms in the graphene sheets [14].

Many theories have already been developed to calculate the particle distribution in a confined space [1]. Essentially, the particle distribution can be determined by minimizing the Helmholtz free energy [15]. However, since the free energy is a functional of the particle distribution and its exact definition is difficult to formulate, appropriate models must be introduced. For a confined hard-sphere fluid, the density profiles predicted by the Tarazona model [16,17] agree with Monte Carlo simulations with fixed walls. In contrast, models able to predict the density profiles of particles located between flexible walls have not been sufficiently developed. Thus, in this study, we used MD simulations [18] to calculate the density profiles of particles confined between graphene sheets.

Although the fabrication of large suspended graphene sheets with current technologies is a difficult task, a narrow space can be probably created by locating small suspended graphene sheets, which are fabricated above small pits, in parallel with a finite gap [10,19]. Therefore in this study we investigate a Lennard-Jones system confined between nanographene sheets. In addition, the fundamental frequency of graphene sheets increases as their size decreases, and graphene is rapidly deformed upon application of an external force. This feature facilitates the use of MD simulations for finding the stable particle distributions. Conversely, the layer structure of a molecule, which is the main focus in this study, is hard to form for larger-area graphene sheets due to the large horizontal fluctuation of graphene sheets.

This paper is structured as follows. In Sec. II, we analyze the density profiles of argon atoms confined between fixed graphene sheets separated by different separation distances. Each argon atom interacts with other argon atoms, as well as with the carbon atoms of the graphene sheets. For small separations, the particle density profile perpendicular to the graphene surfaces reaches a maximum at the center, whereas two peaks appear for large separations. This change in density profile is qualitatively explained by considering the stability of the particles near the center of the gap separating the graphene sheets. In Sec. III, we investigate the density profiles of particles confined between graphene sheets, in which all carbon atoms are mobile except those located along the sheet edges. In particular, we discuss the effects of changing the boundary conditions. In Sec. IV, we calculate the density profiles of the particles starting from a cluster located between graphene sheets separated by large distances; in this case, we discuss the

_____
[*]inui@eng.u-hyogo.ac.jp

formation of a liquid droplet on a graphene sheet and the structure of a bridge formed between two sheets. Finally, in Sec. V, we summarize the results of the MD simulations and discuss several issues that should be addressed in future studies.

II. DENSITY PROFILES OF PARTICLES CONFINED BETWEEN FIXED GRAPHENE SHEETS

We consider a Lennard-Jones system in which the potential energy of interaction is expressed as

$$V(r) = 4\epsilon \left[\left(\frac{\sigma}{r} \right)^{12} - \left(\frac{\sigma}{r} \right)^6 \right] \tag{1}$$

$$= \epsilon \left[\left(\frac{R}{r} \right)^{12} - 2 \left(\frac{R}{r} \right)^6 \right], \tag{2}$$

where r is the distance between two particles. The above Lennard-Jones potential reaches its minimum at $R = 2^{1/6}\sigma$. The parameters ϵ and σ depend on the constituent elements of the Lennard-Jones system. In this study, we used the ϵ and σ parameters of argon ($\epsilon_{ArAr} = 10.8$ meV and $\sigma_{ArAr} = 3.428$ Å). The interaction potential between an argon and a carbon atom is also represented by the Lennard-Jones potential, with $\epsilon_{ArC} = 6.04$ meV and $\sigma_{ArC} = 3.438$ Å. The interaction energy between an argon and a carbon atom is smaller than that between two argon atoms. However, as the density of carbon atoms is usually larger than that of argon atoms, the interaction energy between an argon atom and a graphene sheet is not always small.

We calculate the density profiles using MD simulation in the NVT (constant number of particles, volume, and temperature) ensemble. Figure 1 shows two initial configurations used in the simulations. In the 2D configuration [Fig. 1(a)], 45 argon atoms are located on a triangle lattice parallel to the two graphene surfaces, which are vertically separated by a distance h. The minimum distance between argon atoms in the 2D configuration is $R_{ArAr} = 2^{1/6}\sigma_{ArAr}$. Each graphene sheet consists of 322 carbon atoms and has a rectangular shape with 29 Å×27.62 Å dimensions. We use the Tersoff potential to express the potential energy between carbon atoms in graphene sheets [20,21]. The carbon atoms at the edge of the graphene sheet (100 in total) are fixed. Armchair and zigzag edge configurations are used along the x and y axes, respectively. The argon cluster consists of 45 atoms and its details are discussed in Sec. III.

To consider the probability density of finding a particle, we introduce the normalized vertical position of an argon atom defined by

$$\zeta \equiv \frac{\min\limits_{i \in \text{lower}} \{z - z_i\}}{\min\limits_{i \in \text{lower}} \{z - z_i\} + \min\limits_{i \in \text{upper}} \{z - z_i\}}, \tag{3}$$

where z and z_i are the z components of the argon atom and of the ith carbon atom in a graphene sheet, respectively. The $\min_{i \in \text{lower}}\{z - z_i\}$ and $\min_{i \in \text{upper}}\{z - z_i\}$ parameters are the minimum vertical distances between the argon atom and the nearest carbon atom in the lower and upper graphene sheets, respectively. The particle density profiles obtained in this way are compared with those calculated for particles confined between flexible graphene sheets. In the latter case, as the distance between an argon atom and the graphene sheets can change, the position of the atom relative to the graphene sheets is more informative than its absolute position.

Figure 2 shows the histogram of the probability density of finding a particle between fixed graphene sheets at a normalized vertical position between ζ and $\zeta + d\zeta$, where $d\zeta = 0.01$. The particle density profiles are calculated for separation distances h between graphene sheets of $2R_{ArAr}$, $2.5R_{ArAr}$, and $3R_{ArAr}$ (displayed from the top to the bottom of the figure). The temperature is 90 K for any separation distances. The Newtonian equations of motion are solved using the Gear method with a time increment Δt of 0.1 fs, and periodic boundary conditions are applied. The maximum number of time steps in the calculations is 5.5×10^6 corresponding to a total MD length $T = 550$ ps, and the Nosé-Hoover algorithm is applied. The positions of the particles are stored every 0.1 ps in the interval from 500 to 5500, where the particle distribution is almost stable. The cutoff length is 100 Å.

For small separations, the particle density reaches its maximum at the center. However, as the separation distance increases, two peaks appear in the density distribution and the particle density at the center significantly decreases. To understand this change in the density profile, we introduce a one-dimensional Lennard-Jones system, consisting of three
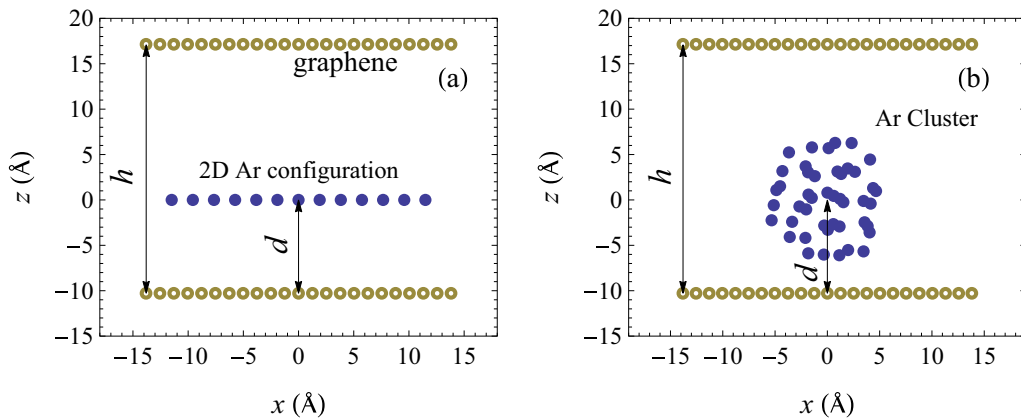

FIG. 1. Initial configurations of argon atoms (blue filled circle) confined between carbon atoms (brown open circle): (a) two-dimensional and (b) cluster configurations.
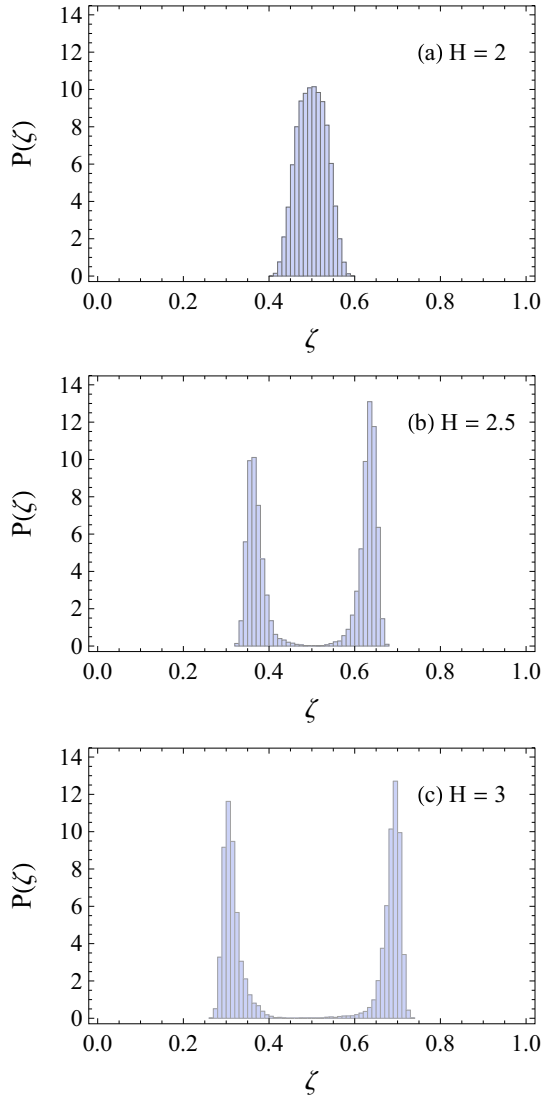
FIG. 2. Density profiles of argon atoms as a function of the normalized distance from the lower graphene sheet for different normalized separation distances H.

particles arranged along the x axis. The first and second particles are located at $-h/2$ and $h/2$, respectively. If the third particle is located at x, the total potential energy is given by

$$U(x, h) = V(x) + V(x - h) + V(h). \tag{4}$$

Figure 3 shows $U(x, h)$ as a function of the normalized position x/R_{ArAr} for different normalized separation distances $H = h/R_{\text{ArAr}} = 2.0, 2.1, \ldots, 2.6$. For small H values, the total potential energy reaches a minimum at the origin, i.e., halfway between the first and the second particle. As H increases, the potential energy at the origin increases and the second derivative at the origin becomes zero at $H_c = 2(13/7)^{1/6}(=2.217)$. For $H > H_c$, the particle at the origin is unstable and two stable positions are observed. The curvature at the origin increases as H approaches H_c from zero. This means that the standard deviation of the particle density increases near H_c.

Similar changes in the potential energy are observed for the Lennard-Jones system sandwiched between graphene sheets.
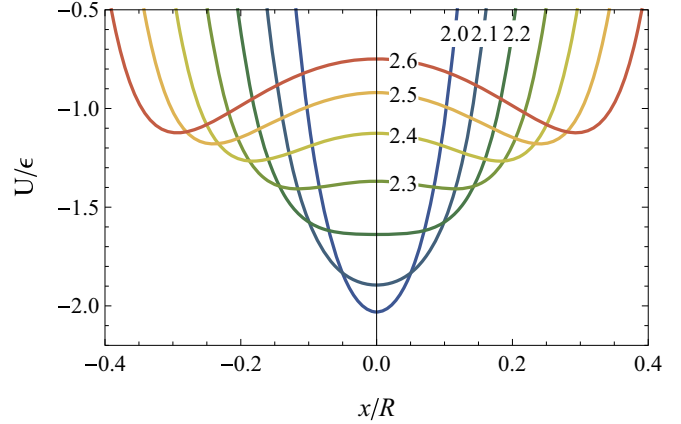

FIG. 3. Potential energy profile for a linear arrangement of three atoms, positioned at $-h/2$, $h/2$, and x. The numbers shown in the figure denote $H = h/R$ values. The second derivative at $x = 0$ changes from positive to negative when $H > 2.22$.

Figure 4 shows the potential energy of the Lennard-Jones system whose configuration is shown in Fig. 1(a) as a function h. In Fig. 5 the stable positions z_s where the potential energy reaches the minimum are shown. Although the carbon atoms in the graphene sheets are fixed in this part of the calculation, the distance between argon atoms is determined so that the potential energy is minimized. Only one stable position, located at the center, i.e., $h/2$, is found for $h \leqslant 7.8$ Å ($\approx 2R_{\text{ArAr}}$). Two stable positions appear for $h > 7.8$ Å, one near the lower graphene sheet, and the other near the upper graphene sheet. The difference in the particle distributions shown in Figs. 2(a) and 2(b) is qualitatively explained by the change in the corresponding potential energies.

III. DENSITY PROFILES OF PARTICLES CONFINED BETWEEN FLEXIBLE GRAPHENE SHEETS

It is well known that a suspended graphene sheet can be easily bent by the application of an external force [22]. Thus, we examine the change in the distribution of argon atoms
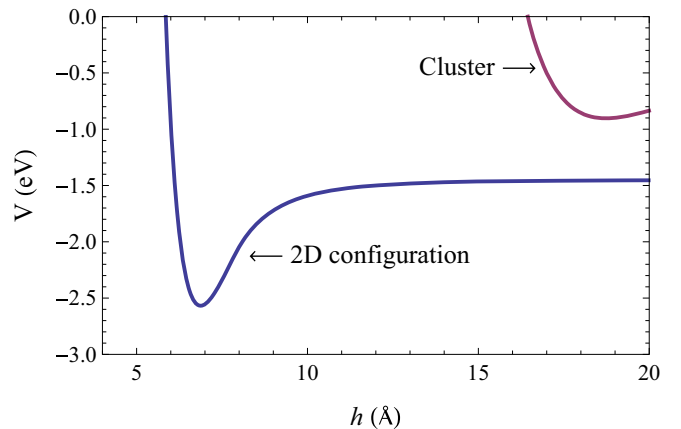

FIG. 4. Potential energies of argon atoms arranged in 2D and cluster configuration as a function of the separation between graphene sheets. Both configurations are located halfway between the graphene sheets.
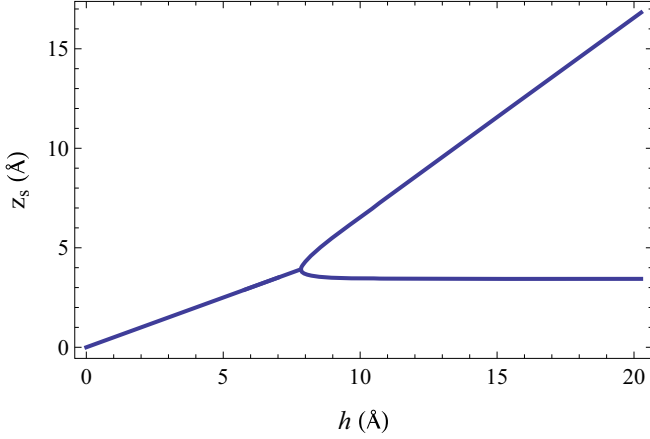
FIG. 5. Vertical stable position of argon atoms initially arranged in a 2D configuration. A bifurcation occurs near the separation distance $h = 7.8$ Å ($= 2.0 \, R_{ArC}$).

between graphene sheets caused by the deformation of the latter. Figure 6 shows the histogram of the probability density of particles confined between flexible graphene sheets. The simulation conditions are the same as those applied in Sec. II except for the flexibility of the graphene sheets.

The most significant difference between the particle density profiles obtained with fixed and flexible graphene sheets is observed for $H = 2.5$ [see Fig. 6(b)]. Two peaks appear in the density profile corresponding to the fixed graphene sheets, whereas a single peak is observed for the Lennard-Jones system confined between flexible graphene sheets. To understand this difference, we introduce the mean distance between graphene sheets, defined by

$$\bar{h} = \frac{1}{t_2 - t_1} \int_{t_1}^{t_2} \frac{1}{N} \sum_{i=1}^{N} |z_{i,\text{upper}}(t) - z_{i,\text{lower}}(t)| dt. \quad (5)$$

In Eq. (5), N is the number of carbon atoms in a graphene sheet and $z_{i,\text{upper}}(t)$ ($i = 1, 2, \ldots, N$) is the vertical position of the ith carbon atom in the upper graphene sheet at time t. Similarly, $z_{i,\text{lower}}(t)$ denotes the vertical position of the carbon atom in the lower graphene sheets that initially faces the ith carbon atom i in the upper graphene sheet. The obtained mean distance between graphene sheets whose separation distance between the edges $H = 2.5$ is 8.1 Å, which corresponds to $H = 2.1$ for $t_1 = T/2$ and $t_2 = T$. Thus, the separation between graphene sheets decreases in comparison with that in the initial configuration. This is because the graphene sheets move inward due to the attractive force between atoms and buckling occurs. As shown in Sec. II, for small separation distance the potential energy reaches its minimum at the center. Accordingly, only one peak is observed, instead of two. By increasing the length and width of the graphene sheet by 10% with a fixed number of carbon atoms, the tension is increased and the mean distance is suppressed less than 0.1 Å. It follows that two sharp peaks are observed in the distribution profile.

Two shoulders near $\zeta = 0.4$ and 0.6 are observed in Fig. 6(b). To explain this peculiarity in the density profile, Fig. 7 shows the positions of the argon atoms between 90
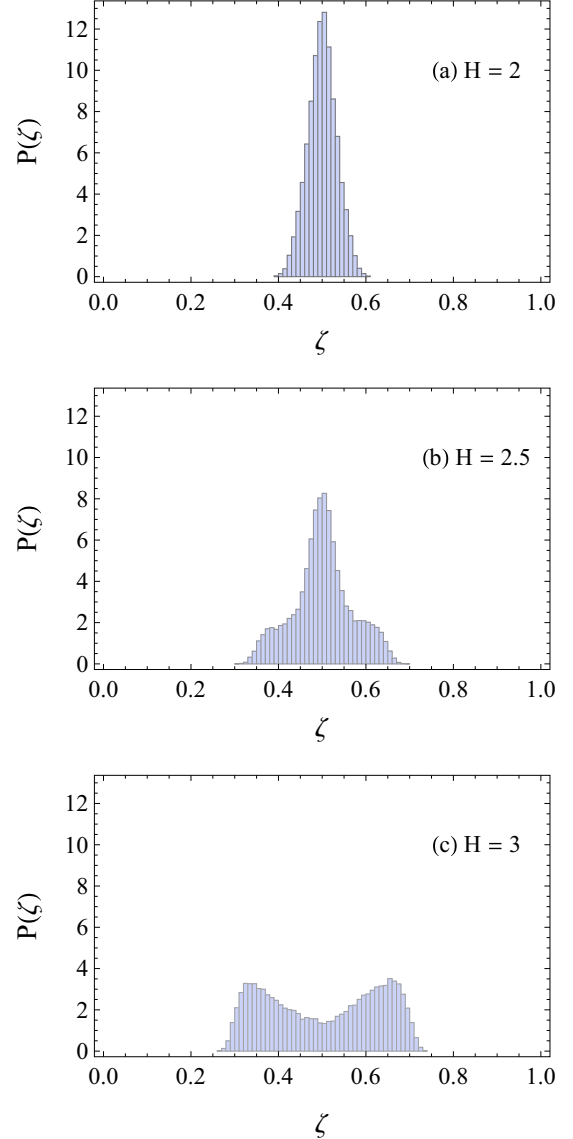

FIG. 6. Density profile of argon atoms confined between flexible graphene sheets at 90 K.

and 100 ps at 0.1-ps intervals. The argon atoms marked with open diamonds (red) are located between $y = -9$ and 9 Å, and the remaining argon atoms, which is marked with solid circles (blue), are located outside the region between $y = -9$ and 9 Å. Argon atoms highlighted with blue solid circles are frequently found near the shoulders in the density profile mentioned above. This means that the particle distribution depends on the y position. Since the edges of each graphene sheet are fixed, the separation between graphene sheets is larger near the edges than around the center. Thus, the vertical distribution near the edge becomes broad and results in the formation of shoulders in the density profile. In other words, the presence of shoulders in the density profile originates from the bending of the graphene sheets.

Figure 6(c) shows that the mean distance between graphene sheets for $H = 3$ is 9.9 Å, which corresponds to $H = 2.6$. Comparing this figure with Fig. 2(b), whose normalized separation distance is $H = 2.5$, two peaks are observed in
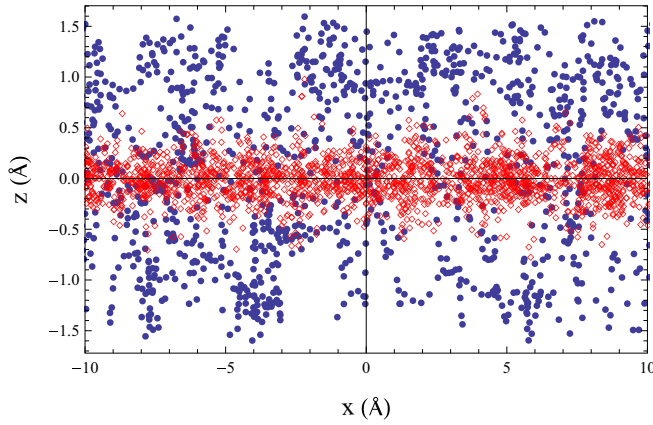
FIG. 7. Superimposed particle positions of argon atoms (whose density profile along the z-axis is shown in Fig. 6(b)) and carbon atoms. The different shapes of the marks denote positions along the y-axis. The argon atoms marked with open diamonds and solid circles are located on the near and far sides of the xy plane, respectively.

both density profiles. However, smaller peaks are obtained for flexible graphene sheets compared with fixed ones, along with a broader particle distribution (extending to the region between the peaks). The vibration of the flexible graphene sheets, which originates in the thermal fluctuation and the collision with argon atoms, alters the sharp particle distribution observed for the fixed sheets. The decrease in the peaks is observed also in the density profile of the system between the 10% stretched graphene sheets.

To consider the temperature dependence of the density profiles, the density profile of argon atoms confined between flexible graphene sheets at 30 K is shown in Fig. 8. A comparison of Fig. 2(b) with Fig. 8(b) reveals that the double peak in Fig. 2(b) disappears and a single peak appears in Fig. 8(b). In addition, a comparison of Figs. 6(b) and 8(b) indicates that more argon atoms at 30 K are closely packed near the center.

IV. VELOCITY DISTRIBUTION, PRESSURE, AND AVERAGE MEAN SQUARE DISPLACEMENT

The ratio of surface area to volume in a confined system is larger than that in a bulk system. Therefore, the thermal vibration of graphene sheets may greatly affect the velocity distribution of argon atoms between them. Figure 9 shows the velocity distribution of argon atoms confined between flexible graphene sheets (blue dots) and the carbon atoms of the flexible graphene sheets (green dashed line) for different separation distances of the graphene sheets. The red squares in Fig. 9 show the velocity distribution of argon atoms confined between fixed graphene sheets and the red solid line represents the Maxwell distribution of atoms whose mass is equal to that of argon at 90 K. The velocity distributions of argon atoms confined between fixed graphene sheets obey the Maxwell distribution independently for the separation distance. However, the velocity distribution of argon atoms confined between flexible graphene sheets is different from the Maxwell distribution, and is rather close to the distribution of carbon atoms in flexible graphene. The argon atoms frequently collide with the graphene sheet, and the number density of carbon atoms
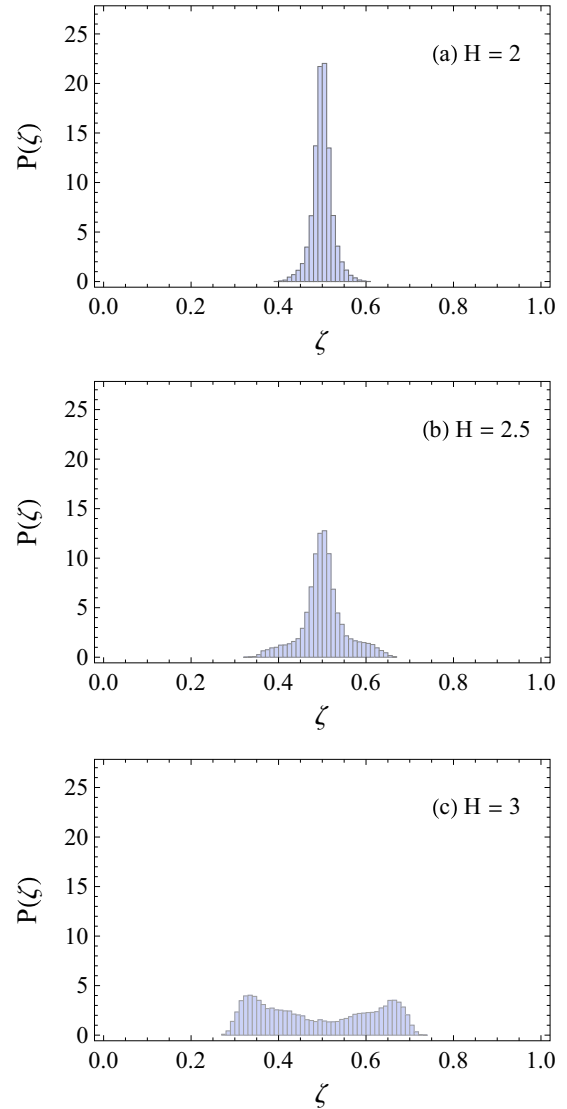

FIG. 8. Density profile of argon atoms confined between flexible graphene sheets at 30 K.

per area is higher than that of argon atoms. Thus, the velocity distribution of carbon atoms reflects that of argon atoms.

Figure 10 shows the change in the pressure acting on the graphene sheet versus time for (a) fixed and (b) flexible graphene sheets at 90 K. The simulation method was changed from NVT to NVE at $t = 10$ ps. For both methods, a large fluctuation is observed for the flexible graphene sheets. This is consistent with the fact that the velocity distribution of argon atoms confined between flexible graphene sheets is broad in comparison with the Maxwell distribution of atoms at 90 K.

A similar difference caused by the change in boundary conditions is observed for the mean square displacement. Figure 11 shows the mean square displacements within 5 ps averaged over ten different initial configurations for (a) fixed and (b) flexible graphene sheets at 90 K. Although the calculation time is too short to determine the diffusion coefficient, the simulation result suggests that the argon atoms confined between flexible graphene sheets are more quickly diffused than those confined between fixed graphene sheets. In addition, the
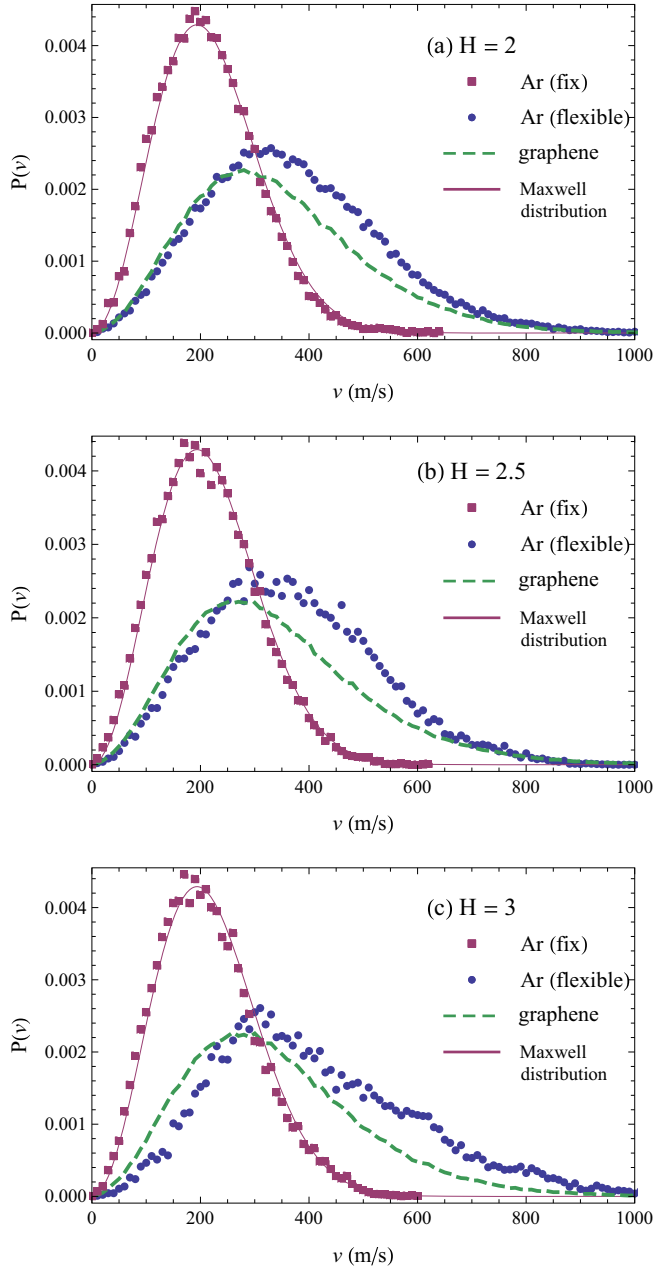
FIG. 9. Velocity distribution of argon atoms and carbon atoms confined between graphene sheets with the separation distance $H = 2$, 2.5, and 3 (from top to bottom). The red square and red line show the velocity distribution of argon atoms confined between fixed sheets obtained from the MD simulation and Maxwell distribution at 90 K, respectively.

mean square displacement increases more rapidly for large separation distances. This is probably because the density of argon atoms in each layer is lower for large separation distances.

V. DENSITY PROFILES FOR LARGE SEPARATIONS BETWEEN NANOSHEETS

The layered structure of argon atoms parallel to the graphene sheets is most stable for small separations. However,
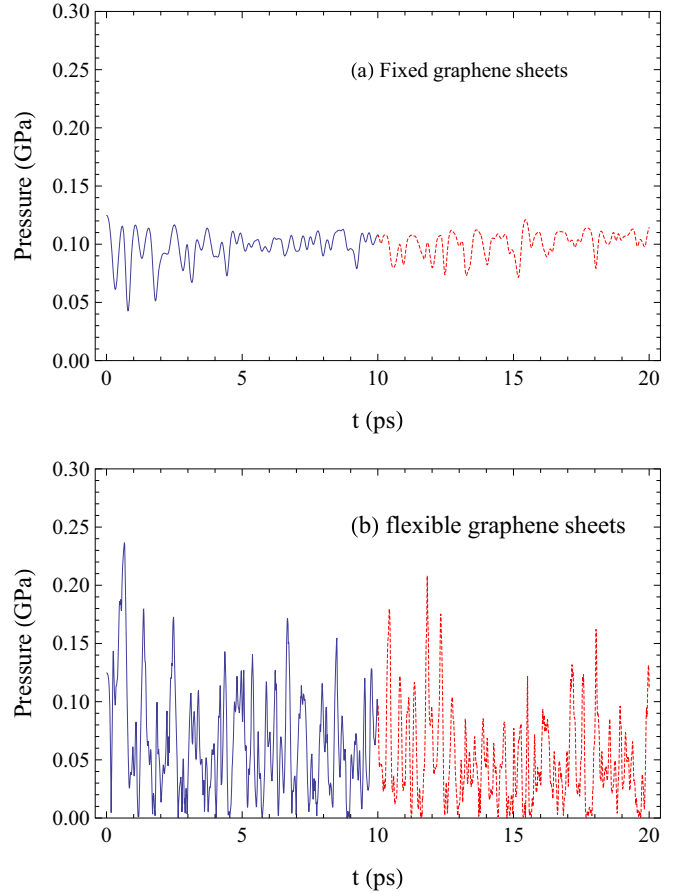

FIG. 10. Temporal dependence of the pressure acting on a fixed and flexible graphene sheet. The condition of the ensemble was changed from NVT to NVE at 10 ps.

various metastable configurations are allowed for large separations. For example, an argon cluster can persist for a long time, if sufficiently separated from the graphene sheets. In Fig. 4, the minimum potential energy of a cluster consisting of 45 argon atoms is plotted as a function of the separation between the graphene sheets. The initial configuration of the argon atoms is illustrated in Fig. 1(b). For any separation, the potential energy for the system including the cluster is larger than that of the 2D configuration with argon atoms arranged parallel to the graphene sheets. Thus, the argon cluster must change shape when it approaches the graphene sheets.

After positioning an argon cluster at $d = 12$ Å above a graphene sheet [see Fig. 1(b)], the density profile is calculated using the same simulation conditions described in Sec. II, with the exception of the separation distance and temperature. In particular, the separation distance is set to $10R_{ArAr}$ and the temperature is changed from 90 to 30 K. Figure 12 shows the superimposed positions of all argon atoms in the x-z plane, collected from 50 and 100 ps at $1000\Delta t$ intervals. The x_r and z_r coordinates denote the position of an atom relative to the center of mass of the all argon atoms along the x and z axes at each time, respectively. The black and gray filled circles denote the positions of argon and carbon atoms, respectively. A droplet structure is observed to form on a graphene sheet.
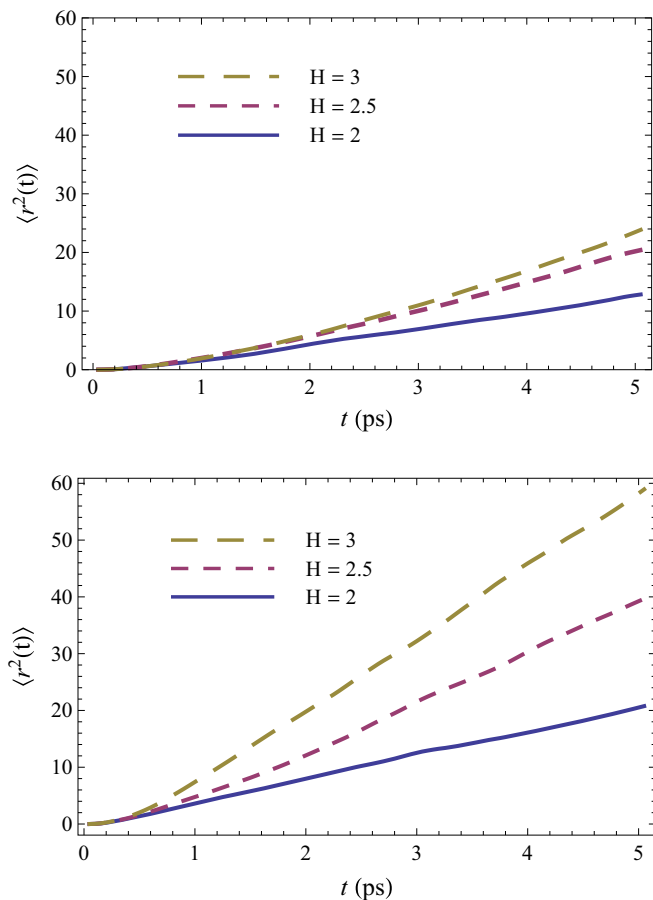
FIG. 13. Superimposed positions of argon and carbon atoms confined between flexible graphene sheets for $H = 10$ at 30 K.

those used to obtain Fig. 12. The argon atoms are distributed almost uniformly on the graphene surfaces and some atoms occasionally cross the space between the graphene sheets. The comparison with Fig. 12 suggests that the vibration of the graphene sheets prevents the formation of the droplet.

The typical interaction length between an argon and a carbon atom is $R_{ArC} = 3.86$ Å. If $h \gg R_{ArC}$, the interaction between argon atoms and the carbon atoms in either the upper or lower graphene sheets is very weak. The configurations in Figs. 12 and 13 correspond to this case. The motion of argon atoms is mainly governed by the interaction with the nearest graphene sheet. Conversely, when the separation distance is almost equal to the cluster height (12.4 Å), the argon atoms near the top (bottom) of the cluster strongly interact with the upper (lower) graphene sheet. Thus, the argon cluster is vertically stretched between the two graphene sheets. Figure 14 shows the superimposed positions of argon atoms for $H = 19.24$ Å $(=5R_{ArAr})$ and $T = 1$ K. The top and bottom positions of the cluster touch the graphene surfaces, and a bridge is formed in the space between the graphene sheets. The bridge structure is only observed at low temperature.

FIG. 11. Mean square displacement of argon atoms for (a) fixed and (b) flexible graphene sheets.

The droplet randomly moves on the lower graphene sheet while retaining its shape.

Figure 13 shows the superimposed positions of argon atoms confined between flexible graphene sheets, where the temperature and the separations distance are the same as
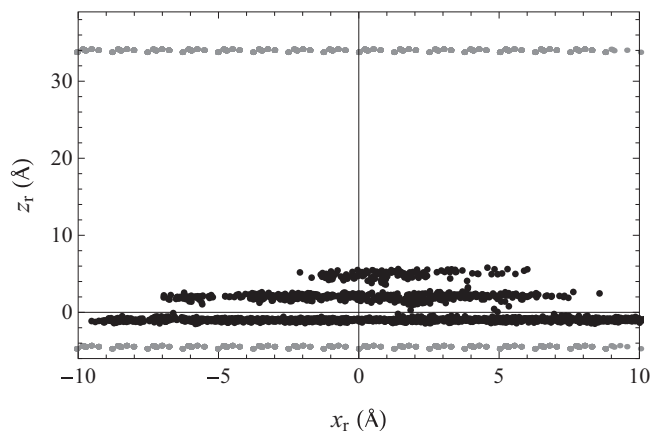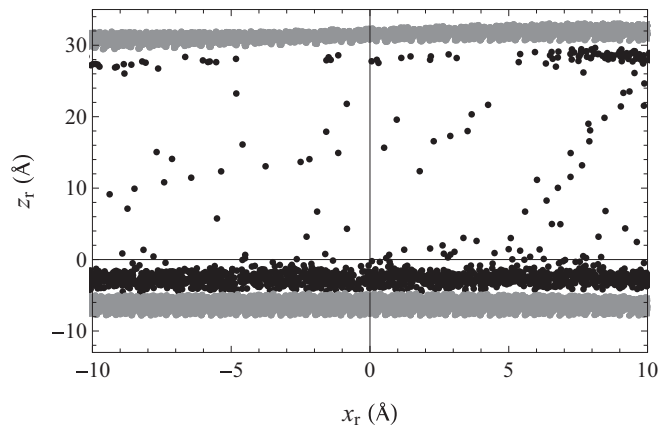

FIG. 12. Superimposed positions of argon (black) and carbon (gray) atoms confined between fixed graphene sheets for $H = 10$ at 30 K; where the origin is set to be at center of mass of the argon atoms.
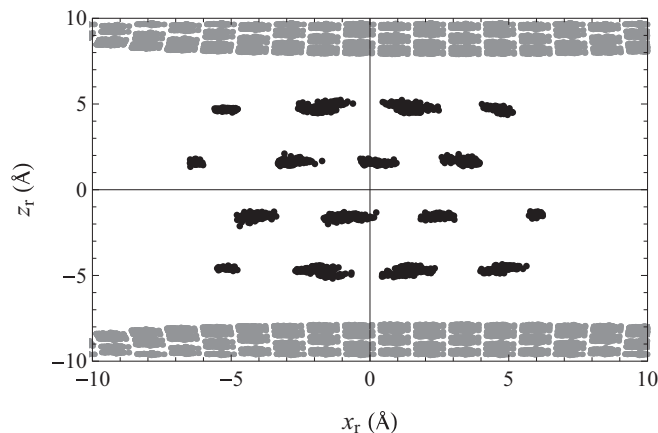

FIG. 14. Bridge structure formed by argon atoms confined between flexible graphene sheets for $H = 5$ at 1 K.

VI. CONCLUSIONS

The most significant property of the Lennard-Jones system sandwiched between graphene sheets is the flexibility of the boundaries. The small bending energy of graphene facilitates changing the distance between the graphene sheets by the application of an external force. We showed that the deformations and fluctuations of the graphene sheets play an important role in determining the layered structure of argon atoms for small separations between the nanosheets. For large separations, the MD simulations yielded several stable arrangements of argon atoms, such as layered structures (wetting) on a graphene sheet, droplets, and bridges, depending on the separation distance, temperature, and initial configuration.

Since the mass of a graphene sheet per unit area is extremely small, its deformation is larger than that of other membranes. However, if the residual stress of suspended graphene sheets at fabrication is very large, the deformation of the graphene sheets is very small and the distribution profiles of the confined atoms are approximately equal to those obtained assuming the fixed boundary conditions. The difference in the density profile between the fixed and the flexible boundary condition is primarily caused by the vibration of graphene sheets. Unlike rigid boundaries, a single graphene sheet is locally deformed by the collision with argon atoms, and its deformation affects the distribution of the atoms between graphene sheets.

We described the features of a Lennard-Jones system confined in a narrow space with flexible boundaries, compared with the system sandwiched between rigid walls. However, a few issues remain to be addressed. First of all, the phase diagram of the Lennard-Jones system confined between graphene sheets should be determined. In addition, the stability of the configurations observed in the simulations must be further investigated.

In this study, we focused on the distribution of argon atoms between graphene sheets. The deformation of graphene is another important factor, which can be precisely measured by scanning tunneling microscopy. The comparison of the vertical displacements of the graphene sheets measured by experiments and MD simulations may then be used to verify the accuracy of the present results.

[1] T. K. Vanderlick, L. E. Scriven, and H. T. Davis, J. Chem. Phys. **90**, 2422 (1998).

[2] A. Patrykiejew, L. Salamacha, and S. Sokolowski, J. Chem. Phys. **118**, 1891 (2003).

[3] R. Evans, M. C. Stewart, and N. B. Wilding, J. Chem. Phys. **147**, 044701 (2017).

[4] H. K. Christenson, J. Phys.: Condens. Matter **13**, R95 (2001).

[5] Y. Maniwa, H. Kataura, M. Abe, S. Suzuki, Y. Achiba, H. Kira, and K. Matsuda, J. Phys. Soc. Jpn. **71**, 2863 (2002).

[6] G. Cicero. J. C. Grossman, E. Schwegler, F. Gygi, and G. Galli, J. Am. Chem. Soc. **130**, 1871 (2008).

[7] M. Raju, A. van Duin, and M. Ihme, Sci. Rep. **8**, 3851 (2018).

[8] J. C. Meyer, A. K. Geim, M. I. Katsnelson, K. S. Novoselov, T. J. Booth, and S. Roth, Nature (London) **446**, 60 (2007).

[9] C. Lee, X. Wei, J. W. Kysar, and J. Hone, Science **321**, 385 (2008).

[10] J. S. Bunch, S. S. Verbridge, J. S. Alden, A. M. van der Zande, J. M. Parpia, H. G. Craighead, and P. L. McEuen, Nano Lett. **8**, 2458 (2008).

[11] K. Shi, K. Gu, Y. Shen, D. Srivastava, E. E. Santiso, and K. E. Gubbins, J. Chem. Phys. **148**, 174505 (2018).

[12] R. Mu, Q. Fu, L. Jin, L. Yu, G. Fang, D. Tan, and X. Bao, Angew. Chem. Int. Ed. **51**, 4856 (2012).

[13] Y. Wei, B. Wang, J. Wu, R. Yang, and M. L. Dunn, Nano Lett. **13**, 26 (2013).

[14] S. C. Pradhan, Phys. Lett. A **373**, 4182 (2009).

[15] M. Ross, J. Chem. Phys. **71**, 1567 (2008).

[16] P. Tarazona, Mol. Phys. **52**, 847 (1984).

[17] P. Tarazona, Phys. Rev. A **31**, 2672 (1985).

[18] Y. Kataoka and Y. Yamada, J. Comput. Chem. Jpn. **13**, 115 (2014).

[19] D. Metten, F. Federspiel, M. Romeo, and S. Berciaud, Phys. Rev. Appl. **2**, 054008 (2014).

[20] J. Tersoff, Phys. Rev. B **39**, 5566 (1989).

[21] N. Inui, K. Mochiji, and K. Moritani, Nanotechnology **19**, 505501 (2008).

[22] M. L. Ackerman, P. Kumar, M. Neek-Amal, P. M. Thibado, F. M. Peeters, and S. Singh, Phys. Rev. Lett. **117**, 126801 (2016).